

Gap collapse and flat band induced by uniaxial strain in $1T\text{-TaS}_2$

C. W. Nicholson ^{1,2,*} F. Petocchi,^{1,3} B. Salzmann,¹ C. Witteveen ^{3,4} M. Rumo ¹
G. Kremer ^{1,5} O. Ivashko,⁶ F. O. von Rohr,³ P. Werner ¹ and C. Monney ¹

¹University of Fribourg and Fribourg Centre for Nanomaterials, Chemin du Musée 3, CH-1700 Fribourg, Switzerland

²Fritz-Haber-Institut der Max-Planck-Gesellschaft, Faradayweg 4-6, D-14195 Berlin, Germany

³Department of Quantum Matter Physics, University of Geneva, 24 Quai Ernest-Ansermet, CH-1211 Geneva, Switzerland

⁴Department of Physics, University of Zurich, Winterthurerstrasse 190, CH-8057 Zurich, Switzerland

⁵Institut Jean Lamour, UMR 7198, CNRS-Université de Lorraine, Campus ARTEM, 2 allée André Guinier, BP 50840, 54011 Nancy, France

⁶Deutsches Elektronen-Synchrotron DESY, Notkestrasse 85, Hamburg D-22607, Germany



(Received 23 April 2023; revised 24 October 2023; accepted 22 December 2023; published 31 January 2024)

Interlayer coupling is strongly implicated in the complex electronic properties of $1T\text{-TaS}_2$. Uniaxial strain engineering offers a route to modify this coupling in order to elucidate its interplay with the electronic structure and electronic correlations. Here, we employ angle-resolved photoemission spectroscopy (ARPES) to reveal the effect of uniaxial strain on the electronic structure in $1T\text{-TaS}_2$. The gap of the normally insulating ground state is significantly reduced, with a correlated flat band appearing close to the Fermi level. Temperature-dependent ARPES measurements reveal that the flat band only develops below the commensurate charge density wave (CCDW) transition, where interlayer dimerization produces a band insulator in unstrained samples. Electronic structure calculations suggest that the correlated flat band is stabilized by a modified interlayer coupling of the Ta d_{z^2} electrons. Further hints of a strain-induced structural modification of the interlayer order are obtained from x-ray diffraction. Our combined approach provides critical input for understanding the complex phase diagram of this platform material for correlated physics.

DOI: [10.1103/PhysRevB.109.035167](https://doi.org/10.1103/PhysRevB.109.035167)

I. INTRODUCTION

The overlap between electronic wavefunctions on neighboring atomic sites determines the kinetic energy, or bandwidth, of electronic states in solids. Reducing this overlap to produce narrowly dispersing electronic bands promotes correlated behavior in the presence of electronic interactions [1,2]. This can have particularly striking effects in low-dimensional materials, as exemplified by the milestone discoveries of the fractional quantum Hall effect [3] and high- T_c superconductivity in the cuprates [4]. In layered (quasi-2D) materials, the out-of-plane coupling is typically weaker than that in the plane. Nevertheless, coupling along the out-of-plane direction can play a crucial role in the overall energetics of a material. This manifests, for example, in twisted bilayer graphene, where modified interlayer coupling leads to emergent strongly correlated phases [5,6] and flat electronic bands [7]. Indeed, the higher sensitivity of interlayer coupling to external perturbations provides a control parameter to modify correlated electron behavior. Pressure-induced and -enhanced supercon-

ductivity is well known in numerous 2D layered compounds, and has recently been in focus due to the bulk Kagome series AV_3Sb_5 [8], which hosts diverse phenomena tuneable with pressure [9] and interlayer ordering [10]. Access to the momentum-resolved electronic structure with techniques such as ARPES is required to fully characterize and understand these phenomena, but is hampered by a lack of compatibility between high-pressure cells and surface sensitive techniques.

Uniaxial strain engineering can overcome these limitations, by modifying crystal structures and hence the electronic kinetic energy in the Hamiltonian without constraining access to the sample surface. This approach has proved highly successful in correlated oxides [11–15]. Strain has furthermore been shown to produce effects equivalent to moiré engineering [16,17] and therefore offers a route to control interlayer coupling and emergent properties in a broad range of materials. However, relatively little work on strain engineering in quasi-2D correlated materials has been performed, and the combination with ARPES remains challenging and limited [18–21].

Layered $1T\text{-TaS}_2$ hosts a particularly rich and controversial phase diagram, and has therefore become an important platform material for studying electronic correlations in low dimensions. In addition to a series of charge density wave (CDW) phases upon cooling—with incommensurate (550 K), nearly commensurate (350 K) and commensurate (180 K) structures [22]— TaS_2 also displays superconductivity under pressure [23], a metastable hidden phase following pulsed excitation [24,25], is a candidate quantum spin liquid [26],

*cw_nicholson@protonmail.com

Published by the American Physical Society under the terms of the [Creative Commons Attribution 4.0 International](https://creativecommons.org/licenses/by/4.0/) license. Further distribution of this work must maintain attribution to the author(s) and the published article's title, journal citation, and DOI. Open access publication funded by the Max Planck Society.

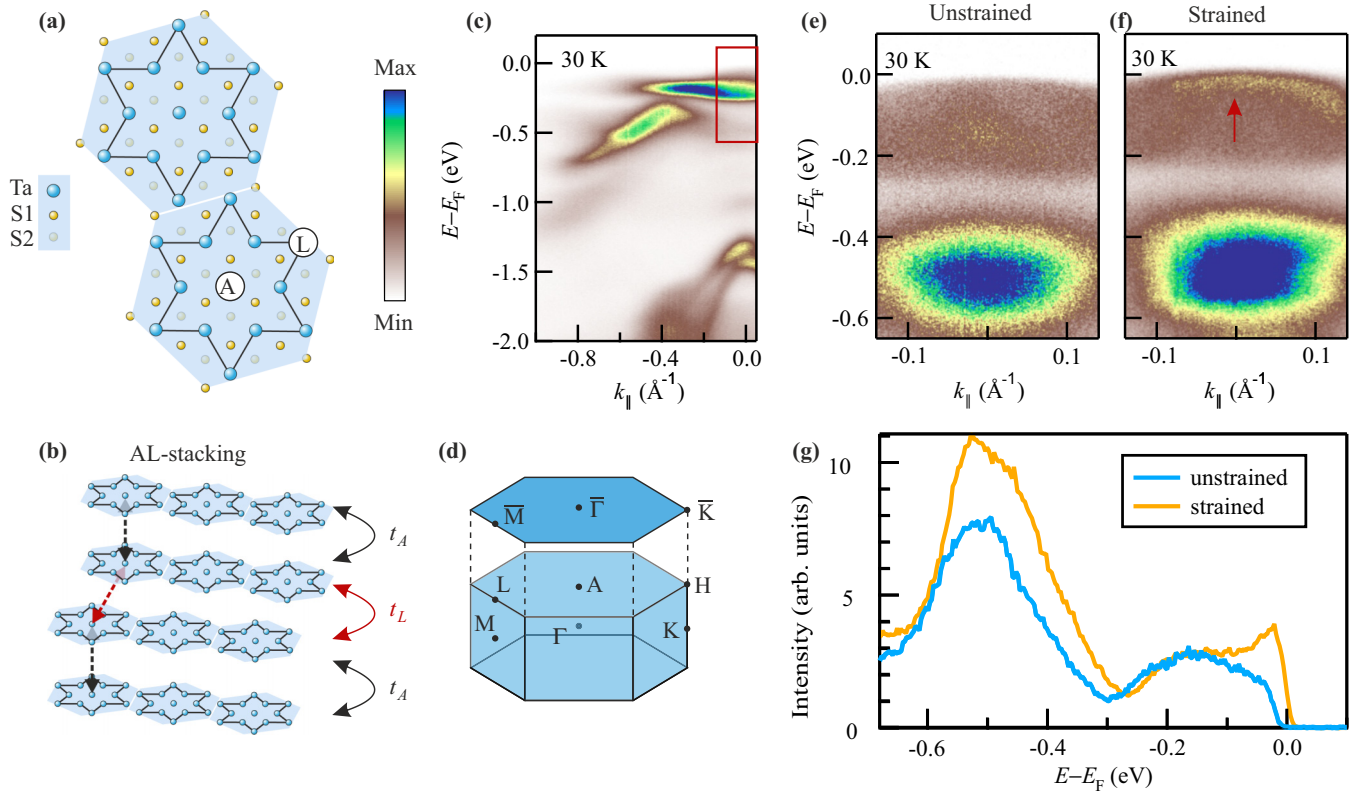


FIG. 1. (a) Top-down view of the TaS₂ surface highlighting the atoms involved in the star-of-David structural rearrangement in the CCDW phase. The central atom A carries the Mott electron in a d_{z^2} orbital. The Ta atom in the outer shell is designated L in line with the previous convention [32]. (b) The equilibrium stacking arrangement in the CCDW phase: bilayers form with the A atoms vertically aligned. Between bilayers the A and one of the symmetry equivalent L atoms are randomly aligned. (c) Photoemission spectra obtained along the $\bar{\Gamma}$ - \bar{M} direction of the surface Brillouin zone shown in (d) at 30 K and with 21.2 eV photon energy. The red box highlights the region probed in (e) and (f). [(e),(f)] Photoemission spectra obtained with 6.2 eV photons for an unstrained and uniaxially strained sample under otherwise the same conditions. The strain-induced flat band is highlighted by the red arrow. (g) Line cuts through the data in (e) and (f) integrated over $\pm 0.036 \text{ \AA}^{-1}$ around the $\bar{\Gamma}$ point.

and hosts a controversial Mott phase in the commensurate CDW (CCDW) phase that has been debated for almost 50 years [27–29]. Recently this debate has intensified [30–34], motivated in part by the fact that doped Mott insulators represent the prototypical framework for understanding high- T_c superconductivity in the cuprates [35].

The out-of-plane stacking structure of TaS₂ along the c axis is irregular in the proposed Mott phase [36,37], with bilayer sheets separated by a randomly assigned off-centre stacking vector [37–40] [see Fig. 1(b)]. An important theoretical step was made when Ritschel [31] and Lee [32] showed that a gapped electronic structure could be obtained via bilayer coupling, as originally suggested by Naito [40]. In a bilayer structure a single electron from each layer can hybridize with the corresponding electron in a neighboring layer and open a bonding-antibonding gap, thus removing the need to invoke Mott correlations. This arises because the star-of-David structures generated by the ionic displacements in the CDW phases contain 13 in-plane Ta atoms, with a total of 12 paired electrons and a single unpaired electron on the central Ta atom in a d_{z^2} orbital [41,42] [see Figs. 1(a) and 1(b)]. However, this implies that a split bilayer created by, e.g., surface termination would result in fundamentally different electronic properties [31]. Recent STM results confirmed that terminations

corresponding to complete and split bilayers are indeed observed [33,34,43]. Moreover both surfaces were found to be gapped; an unexpected result within the single-particle picture. This suggests that at least one termination contains Mott physics, as highlighted by recent calculations [44]. However, in the bulk material any possible Mott correlations are hard to observe due to the presence of the hybridization gap

This begs the question: What happens to the electronic properties if the interlayer stacking is modified away from the ground state and the bilayer structure is disturbed? This is critical information considering that superconductivity appears when the system is pushed away from standard equilibrium conditions by pressure. Similarly the metallic hidden phase driven by nonequilibrium protocols, for which TaS₂ is the prototypical material, may involve stacking rearrangements [25]. The mechanisms through which these phases occur remain unclear, and direct momentum-resolved electronic structure information is difficult to obtain due to the nature of the techniques involved in producing them. A definitive statement of the role played by electronic correlations and interlayer stacking in 1T-TaS₂ and their relation to the various emergent phases in this material remains elusive.

Here, we follow the modifications of the momentum-resolved electronic structure of 1T-TaS₂ under uniaxial strain.

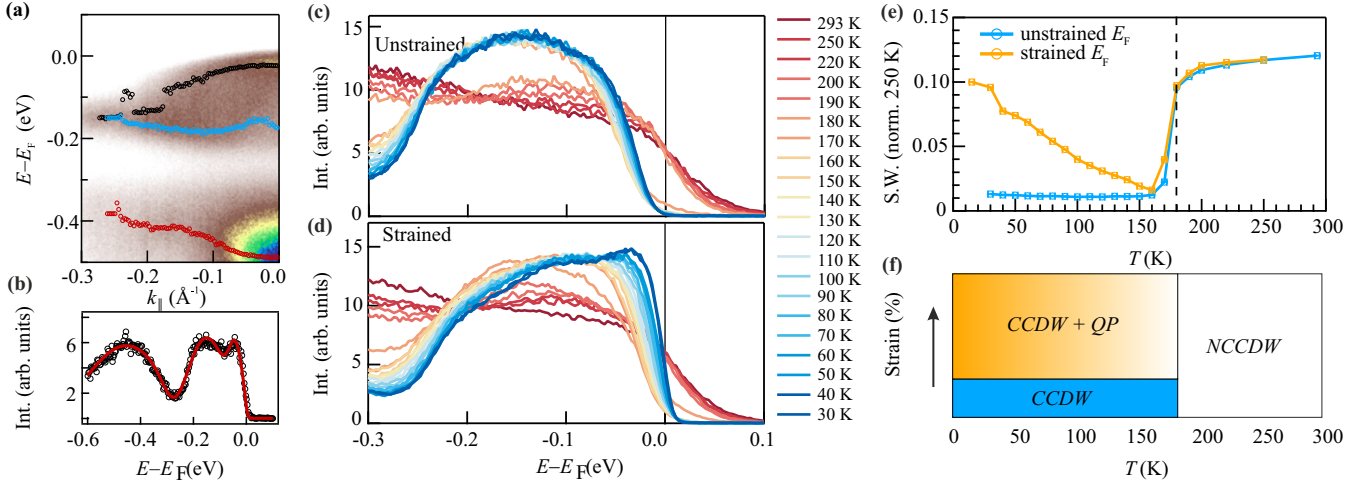


FIG. 2. (a) ARPES data of the strained crystal rotated away from the $\bar{\Gamma}$ point towards \bar{M} . Markers represent the results of a four Gaussian peak fitting multiplied by the Fermi function, a representative example of which is shown in (b). From the extracted dispersion we estimate a bandwidth of 110 meV for the band close to E_F . Due to the rapid loss of spectral weight away from $\bar{\Gamma}$, the fit quality reduces as evidenced by the jump in position at -0.17 \AA^{-1} . [(c),(d)] Line cuts through the photoemission spectra integrated around the $\bar{\Gamma}$ point across the measured temperature range for (c) an unstrained and (d) a strained sample. Note that the data are acquired on a different sample compared to that measured in Fig. 1. (e) Spectral weight as a function of temperature. The curves are obtained for intensity integrated over $[-0.02 : 0.1] \text{ eV}$. The dashed line is the NCCDW to CCDW transition temperature. (f) Schematic phase diagram for strain and temperature.

We demonstrate the appearance of a correlated flat band 20 meV below the Fermi level implying a significant gap collapse compared to an initial gap size of 170 meV in unstrained samples. Structural measurements and electronic structure calculations point to a modification of the interlayer coupling due to strain as the origin of these changes. Our results highlight the interplay between interlayer coupling and electronic correlations in determining the ground state properties of 1T-TaS₂, as well as the possibility of using strain to manipulate electronic properties in layered compounds.

II. RESULTS

The electronic structure of an unstrained TaS₂ crystal in the CCDW phase is presented in Fig. 1(c) along the $\bar{\Gamma}$ – \bar{M} direction of the surface Brillouin zone [Fig. 1(d)]. The Ta 5*d* manifold extends from E_F to -1.5 eV , with S 2*p* states at lower energies [41,42]. These data obtained with 21.2 eV excitation energy are in excellent agreement with previous reports [41,45,46], as are the corresponding transport and structural properties, which are presented in Fig. 6 in the Appendix.

Utilising a low-energy laser source (see Appendix) to focus on the energy region in the vicinity of the Fermi level near the $\bar{\Gamma}$ point, we observe a clear splitting of the Ta 5*d* states due to the CCDW phase [Fig. 1(e)], again in line with previous observations [48,49]. However, by introducing uniaxial strain to the same crystal (see Appendix), unexpected additional spectral weight appears close to E_F in a narrowly dispersing band [Fig. 1(f)]. This is further emphasized by the direct comparison of integrated line cuts presented in Fig. 1(g) for unstrained and strained samples. A clear quasiparticle peak is evident 20 meV below E_F only in the strained case. As highlighted in Fig. 2(a) the bandwidth of this state is at most 110 meV, comparable to the flat bands observed recently in twisted bilayer graphene [7,50]. This value is well below

the 200 meV observed in the unstrained CCDW phase as estimated by the width of the peak closest to E_F in Fig. 1(g) (throughout the text we define the gap as the energy between the peak position and the Fermi level, since we do not have access to the conduction band). We note that the differences in spectral weight distribution between Figs. 1(c) and 1(e) result from the photoemission matrix elements of the 13 subbands present in the CCDW phase resulting from the different photon energies and polarizations used to obtain the data.

We have tracked the evolution of this quasiparticle peak as a function of temperature in order to ascertain its relation to the CDW behavior in TaS₂. For the unstrained sample [Fig. 2(c)], the behavior is consistent with previous reports; namely, the metallic NCCDW phase at room temperature abruptly develops a gap at the CCDW transition, thereby removing spectral weight from E_F below 180 K. After straining the same crystal, the evolution below the transition temperature is markedly different. The spectral weight in the vicinity of E_F increases with reducing temperature, with the quasiparticle peak becoming evident below 50 K. The contrast between strained and unstrained samples is highlighted in Fig. 2(e), where the spectral weight integrated at energies above -0.02 eV at each measured temperature is presented. In the strained sample, a small increase of spectral weight is already observed at 150 K, but becomes considerably enhanced as the sample is cooled to 15 K. The trend suggests that spectral weight may further fill the gap at lower temperatures. Although the transition temperature itself appears to be unchanged upon application of strain, changes in the spectral weight distribution are already evident directly below the transition at 170 K. This clearly implies that the quasiparticle behavior sets in only in the CCDW phase, where Mott physics has previously been postulated. The emergence of a narrow quasiparticle peak is evidence for strongly correlated

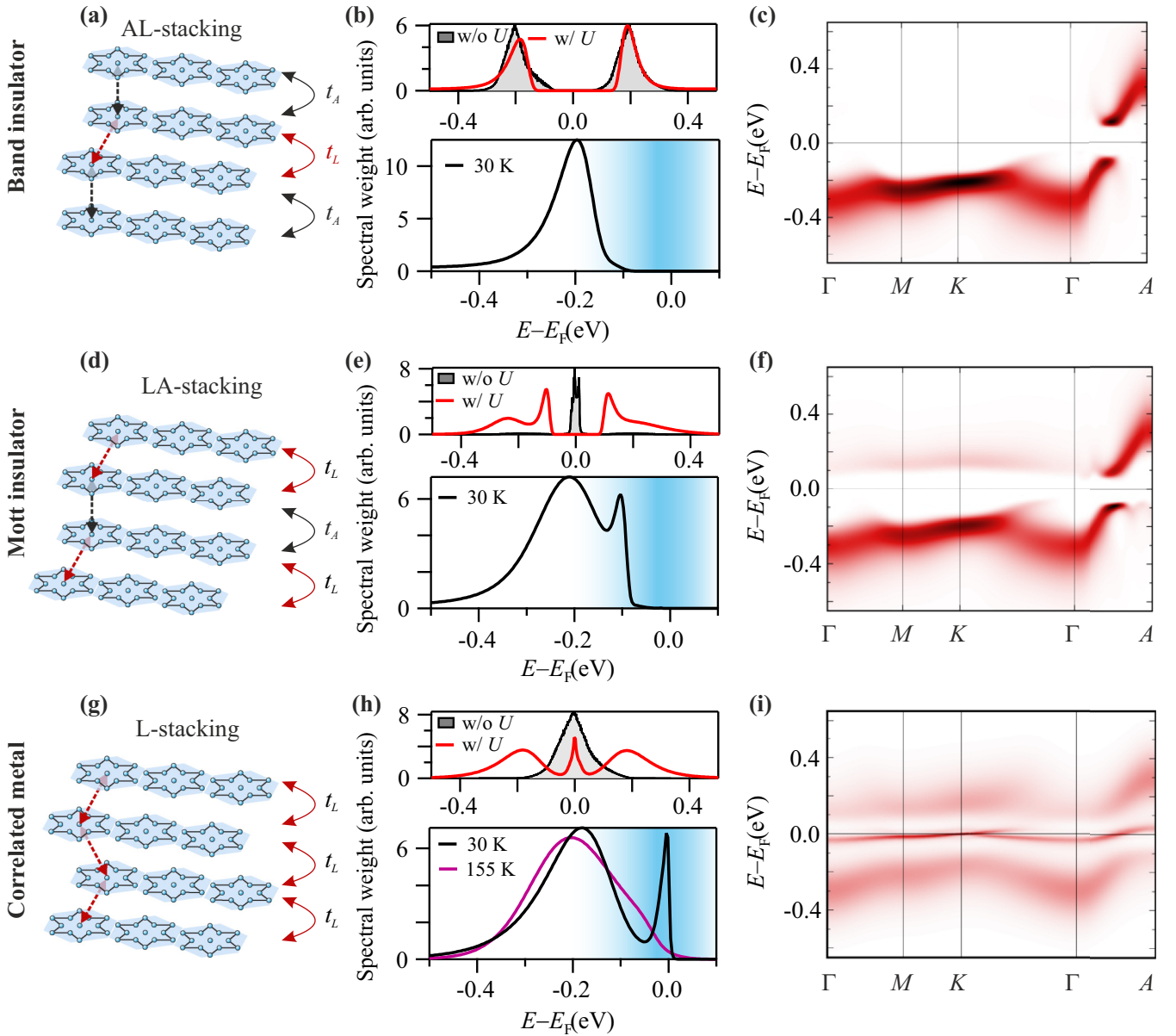


FIG. 3. Electronic behavior for different possible stacking arrangements. (a) The ground-state stacking previously discussed. (b) (Upper) Electronic density of states in the top TaS₂ layer integrated over the in-plane Brillouin zone without (grey) and with (red) electronic correlations included, highlighting the band insulating behavior for this arrangement; (lower) integrated density of states from the first three TaS₂ layers multiplied by the Fermi distribution at 30 K. (c) Calculated spectral function $A(\mathbf{k}, \omega)$ over the full Brillouin zone obtained via the Fourier transform of the relevant real-space dispersions. [(d)–(f)] The same calculations as in [(a)–(c)] for the LA-stacked surface. In this case, the noninteracting structure is metallic [(e), upper] and a Mott gap is opened by electronic interactions [(e), lower]. The Mott gap is smaller than the hybridization gap for the band insulating AL stacking. [(g)–(i)] The same calculations as in [(a)–(c)] for the fully L-stacked system, previously shown to be close in energy to the ground state AL stacking. The metallic quasiparticle appears at 30 K [(h), lower], and is washed out at 155 K, in line with the measured data. The spectral function (i) reveals the flat band throughout the Brillouin zone. Notably the flat band appears at E_F at one-third of the out-of-plane Γ -A distance, compatible with the k_z position expected for 6.2 eV photon energy [47].

physics as it resembles the narrow quasiparticle that appears at E_F in Mott systems in the range where the kinetic energy term (t) and electronic interactions (U) become roughly equal, and which gradually loses coherence with increasing temperature. No additional peak is expected in the gap of a band insulator upon external perturbation of t or U . We note that for both our ARPES and XRD measurements, the same type of sample holder was used as a function of temperature with and without strain applied.

To probe the possible mechanisms involved in the strained samples, we performed GW plus extended dynamical mean-field theory (GW + EDMFT) calculations on a semi-infinite stack of TaS₂ layers (see Appendix) as summarized in Fig. 3. The electronic structure in the lowest energy configuration [Fig. 3(a)], termed AL stacking [32] is characterized by two inequivalent interlayer hopping values between the d_{z^2} orbitals: $t_A = 0.2$ eV within the bilayer, where the stacking vector is $\mathbf{T}_s = \mathbf{c}$, and $t_L = 0.045$ eV between neighboring

bilayers with $\mathbf{T}_s = -2\mathbf{a} + 2\mathbf{c}$. The structure is known to be insulating with a hybridization gap caused by hopping within the bilayer [31,32], and this property is reproduced by our density of states and momentum-resolved spectral function reported in Figs. 3(b) and 3(c) respectively. A second possibility in this AL configuration is to terminate the surface within a bilayer [33,34] [Fig. 3(d)]. As has been recently shown this LA stacked termination is also insulating, but in this case it is strong electronic correlations that open a Mott gap in an otherwise metallic surface state [44] [Fig. 3(e)]. The gap size in the local spectrum of the near-surface region is reduced (100 meV) in this case compared to the AL bulk (200 meV) but the structure remains insulating along all momentum directions [Fig. 3(f)]. Clearly neither of these equilibrium structures (AL or LA stacking) can explain the flat band 20 meV below the Fermi level in strained samples, suggesting the need for a structure where the interlayer hopping is modified.

Since strain adds mechanical energy to the system, we consider as an ansatz the second lowest energy structure [32], with an interlayer stacking as shown in Fig. 3(g). To study this structure we modify the interlayer hopping such that there is equivalent coupling between all layers, with a value of $t_L = 0.035$ eV (see Appendix). This L-stacking structure is very close in energy to the AL-stacking structure, and has been suggested to become the ground state under pressure [32]. Remarkably, the GW+EDMFT calculations [Fig. 3(h)] reveal the appearance of a narrow quasiparticle peak at E_F plus an incoherent background, which qualitatively resembles the structure observed in our ARPES measurements in Figs. 1 and 2. In contrast, the density of states predicted by a noninteracting calculation [Fig. 3(h)] is not consistent with the experimental findings. This is an important result as the role of correlations within the phase diagram of TaS₂ has long been debated. Further evidence for the role of correlations is obtained by increasing the temperature in the GW+EDMFT calculation to 155 K. The fact that this gradually removes the quasiparticle peak, as also observed in the ARPES data of Fig. 2, further highlights the origin of this state in strongly correlated physics, as a noninteracting band cannot be straightforwardly removed by heating. As is evident from Fig. 3(i), the band disperses very narrowly with a bandwidth of only 50 meV at 30 K, comparable to that observed in experiment. The quasiparticle extends into the bulk, as seen in the layer-resolved calculation shown in Fig. 7 in the Appendix. We note that this bulk correlated state in the L-stacking structure contrasts with the correlated Mott gap in the LA structure, which would only appear at surfaces or stacking defects.

The calculated quasiparticle is more clearly separated from the incoherent background than in the experimental data, which suggests that the strain-induced transition is spatially inhomogeneous at the surface and depends on the local strain distribution. Such a scenario would result in a superposition of signals from both AL- and L-stacked structures within the region probed by our laser spot. This is further supported by the data in Figs. 1 and 2, which, although qualitatively similar, show differing relative heights of the quasiparticle peak compared to the background. These independent data sets were obtained on separate crystals and strain devices,

for which the local strain distribution is likely to be different. We therefore postulate the L-stacking structure as a possible mechanism through which the correlated flat band can be produced in strained samples. However, we caution that our model only provides a hypothesis to explain the observed behavior. More involved scenarios combining stacking changes and in-plane variation cannot be ruled out at this stage.

Additional evidence that strain induces a structural change to the bulk crystal is obtained from x-ray diffraction (XRD) measurements shown in Fig. 4. For unstrained samples in the CCDW phase [Fig. 4(a)], broad Bragg peaks centered at -0.18 r.l.u. along the one direction are observed due to the lack of well-defined out-of-plane order, while superstructure peaks at half-order reveal the bilayer stacking associated with this phase [51]. In contrast, strained samples show a clear change compared with the unstrained samples [Fig. 4(b)]. A significant shoulder develops on the superstructure peak in the direction of the out of plane Bragg peak. This suggests an inhomogeneous strain is applied within the 1×1 mm² x-ray spot size, which probes through the entire bulk of the material. An analysis of the distance between the Bragg and superstructure peaks for strained and unstrained samples [Fig. 4(c)], reveals a reduced splitting in the strained case. The splitting originating from applied strain is calculated by an average of the main peak and shoulder, weighted by their relative intensities. The observed reduction of splitting in momentum space implies an increased spacing in real space, i.e., a larger distance between diffraction planes is induced by strain. However, from the peak fitting analysis, we extract no significant change in temperature of the splitting between the main peak and the bilayer satellite. This is an important fact, as it means that once the sample is in the CCDW phase, the structure does not significantly evolve further. In other words, most of the change in the stacking of stars-of-David has already taken place once the transition from the NCCDW to CCDW phase occurs above 180 K. The consequence is that the changes observed as a function of temperature in the electronic structure with ARPES [Figs. 2(d) and 2(e)] are then mostly due to the increased effect of electronic correlations (t/U) in the absence of the bilayer stacking. That being said, a marked increase in the intensity of the shoulder is observed to occur between 150 and 30 K [Fig. 4(d)]. This behavior implies an increased volume fraction of the structural feature contributing to the new shoulder, i.e., the increased tendency towards an L stacking configuration at lower temperatures.

The observed changes in the strained sample offer an indication that the interlayer structure of the CCDW phase is indeed modified by strain, which may in turn lead to a change of the interlayer coupling as proposed in our calculations above. Possible scenarios that explain the observed changes include a real-space increase of the bilayer distance or a movement towards an L-stacking-like structure that includes both in- and out-of-plane components. It is worth mentioning that while metallic features have been observed on cracked samples under strain [52], and within domain walls [53], it seems unlikely that cracks or incoherent domain walls on the nanoscale would lead to a macroscopic band dispersion across tens or hundreds of microns of the sample surface.

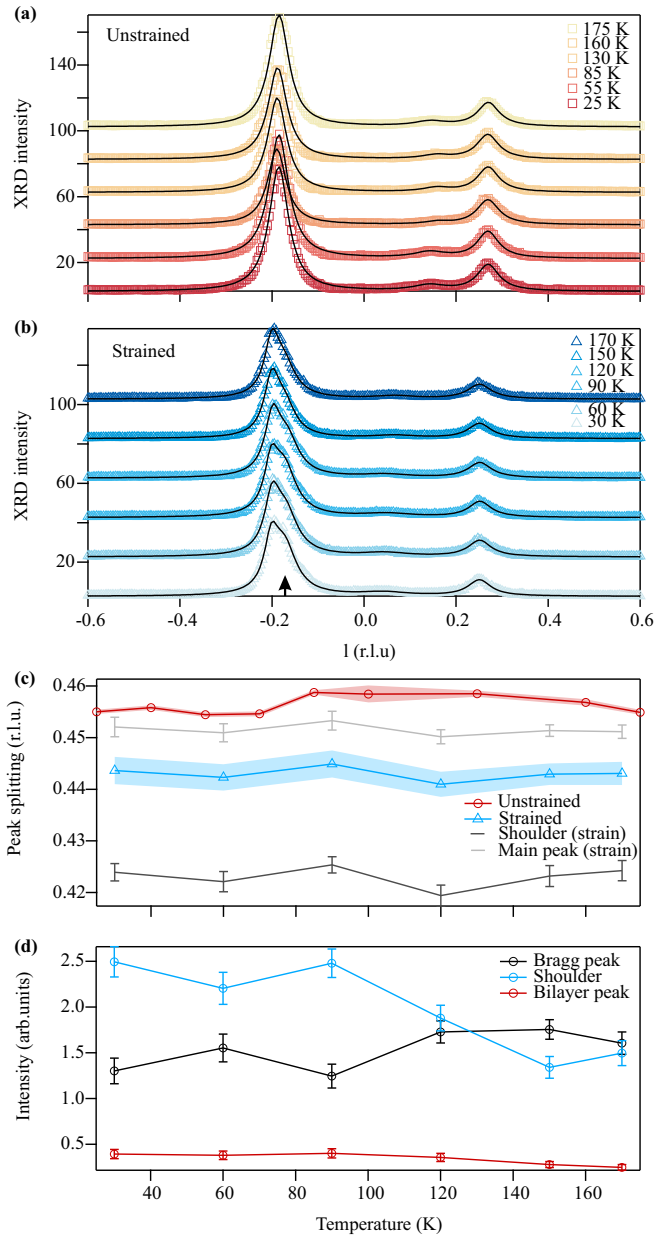


FIG. 4. XRD results for (a) unstrained and (b) strained TaS₂ samples. Solid lines correspond to a Lorentzian peak fitting. (b) Strained samples show a clear change compared with the unstrained samples. (c) Distance between the Bragg and superstructure peaks for strained and unstrained samples, revealing a reduced splitting in the strained case. The strained splitting is calculated by an average of the main peak and shoulder, weighted by their relative intensities. The individual components are also shown in grey. (d) Intensities of the three peaks as a function of temperature extracted from the fit.

III. DISCUSSION

Given the appearance of the flat band below the CCDW transition temperature, it is possible that a partial structural rearrangement occurs during the cooling transition from the NCCDW phase at 180 K in strained samples. According to previous theoretical reports [32], the energy difference between AL and L stacking is only 1.1 meV per star-of-David and the two structures can even become degenerate under

0.3% reduced interlayer spacing, e.g., under pressure. The energy difference between the two phases is likely underestimated, as it implies a significant proportion of L stacking already at temperatures above 10 K, which has not been reported. Regardless of the exact energy values, the fact that the AL and L structures are much closer in energy than all other possible stacking orders supports this as a plausible explanation for the formation of the flat band. This motivates future theoretical investigations of strained TaS₂ samples to better understand the detailed energy landscape induced by strain, as well as more detailed XRD measurements probing the complete structure that occurs in strained samples. We point out that similar considerations are very likely relevant for the Kagome series AV₃Sb₅, where the stacking of star-of-David structural distortions may also play a key role in the energetics of charge ordering [54,55]. Our results imply that strain modifies the interlayer coupling during the NCCDW to CCDW phase transition. It is therefore possible that, at the strain levels applied here, different behavior would be observed for crystals cooled below T_{CCDW} and then strained. It is worth noting that the energy gain through formation of the CCDW phase is on the order of 200 meV per Ta atom [42,46], considerably larger than the estimated changes caused by strain at the current level, meaning we do not expect changes to the in-plane CCDW structure. Changes due to strain may be visible in out-of-plane resistivity measurements, as previously performed on micromachined crystals [56].

A flat metallic d_{z^2} band in TaS₂ has been predicted previously by DFT calculations as a result of spin-orbit coupling, and was postulated as the origin of the Mott phase [42]. However, as discussed above, in the AL-stacked ground state the system is already gapped due to the large interlayer hopping [$t_A = 0.2$ eV, evident from the bandwidth along A in Fig. 3(c)], which causes hybridization and band insulating behavior. While correlations are still present in this structure, they are not responsible for the gap formation and therefore the U is ineffective despite a value of 0.4 eV. In a modified structure, such as the L-stacking structure described above, the interlayer hopping is significantly reduced to only $t_L = 0.035$ eV, thereby removing the hybridization gap [Fig. 3(h)]. This allows the latent Mott correlations to become dominant within the TaS₂ layers. The in-plane bandwidth in the L-stacked structure is around 0.2 eV [Fig. 3(h)], comparable to $U = 0.4$ eV, thereby placing the system in the correlated quasiparticle regime. We remark that the kinetic energy values in our calculations for AL and LA stacking were obtained with reference to previous STM data [33,34]. We note that a similar argument regarding the increased relevance of Mott correlations in an altered stacking arrangement was suggested as an explanation for an insulator-to-insulator transition observed during heating from the CCDW phase [57].

An interesting related material displaying similar physics is 1T-TaSe₂, which also hosts a CDW at low temperatures with strong influence from stacking orders [58]. However, in contrast to 1T-TaS₂ the CDW phase in 1T-TaSe₂ does not show a transition to an insulating phase [22]. The fact that the bandwidth of the valence band in 1T-TaSe₂ is larger (400 meV) compared with that of 1T-TaS₂ (200 meV) in the CDW phase suggests that Mott correlations are weaker in this system. Nonetheless, a recent study has shown that monolayer

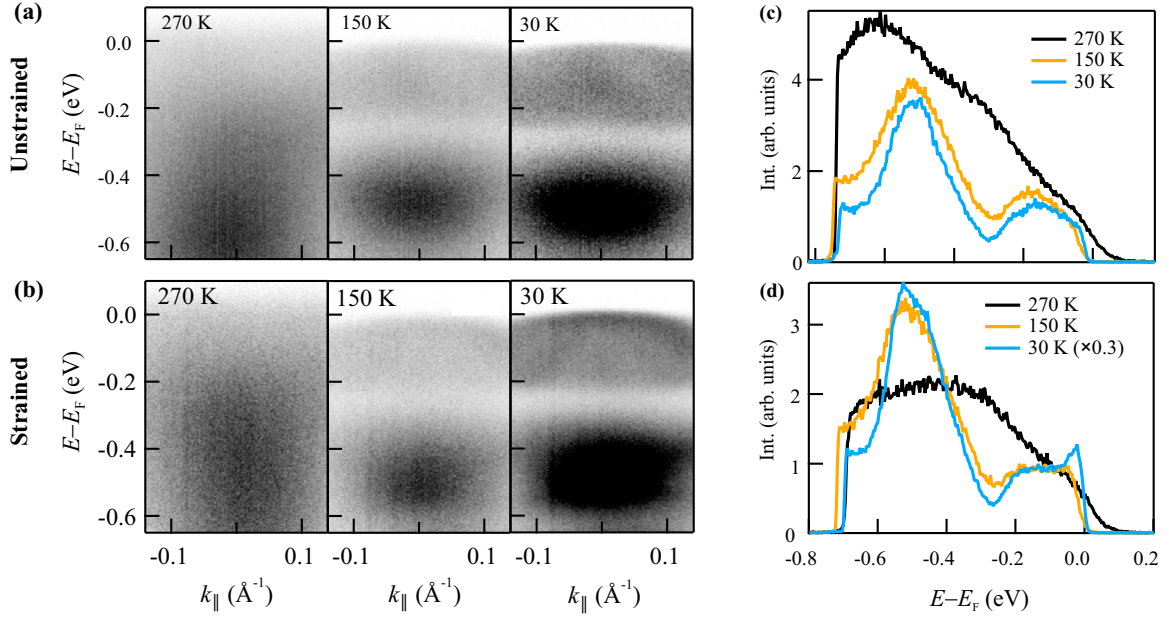


FIG. 5. (a) ARPES spectra at selected temperatures obtained in the $\bar{\Gamma}-\bar{M}$ plane at 6.2 eV in an unstrained crystal at 270 K (NCCDW phase), 150 K (CCDW phase), and 30 K. (b) The corresponding ARPES spectra obtained in the same crystal under strain. The data are obtained on the same crystal as Fig. 1. (c) Line cuts through the unstrained data and (d) through the strained data, highlighting the emergence of the narrow quasiparticle band at E_F .

$1T$ -TaSe₂ is gapped due to Mott correlations [59,60], with this Mott gap reducing and disappearing in bi- and trilayer samples. This suggests $1T$ -TaSe₂ as a potentially interesting material to probe with application of uniaxial strain. We note that in monolayer $1T$ -TaS₂ a spectral gap is observed in tunneling spectroscopy [61], whereas DFT of the monolayer predicts no gap [62].

Intriguingly the behavior observed under strain in the present study does not appear identical to that under hydrostatic pressure [23,63]. Measurements in the CCDW phase under increasing pressure show that the structure initially transitions to the NCCDW phase followed by the onset of superconductivity at higher pressures. Our present results in low-temperature strained samples do not resemble the band structure in the NCCDW phase (see Fig. 5). Nevertheless, the increased relevance of correlations in the strained structure along with the high density of states associated with the flat band may still be relevant to understanding the appearance of superconductivity in TaS₂. Additionally, a strain-induced scenario as outlined above may provide useful in unraveling the mechanism of the metastable hidden phase. STM studies have shown that changes of the interlayer registry can produce local metallic behavior [25,33,52], while XRD has revealed that the dimerized layers of the CCDW phase can be removed by the application of a single picosecond optical pulse [51], although these results do not show evidence for an L-stacked structure in the metastable phase. In general, pulsed optical excitation can produce transient electronic temperatures of the order of 10^3 K, which can in turn induce significant atomic movement due to the altered population of bonding and antibonding states [64]. In the case of TaS₂, a possible scenario would be that optical or electronic pulses produce a nonequilibrium electronic landscape resulting in shifted atomic positions, i.e., an

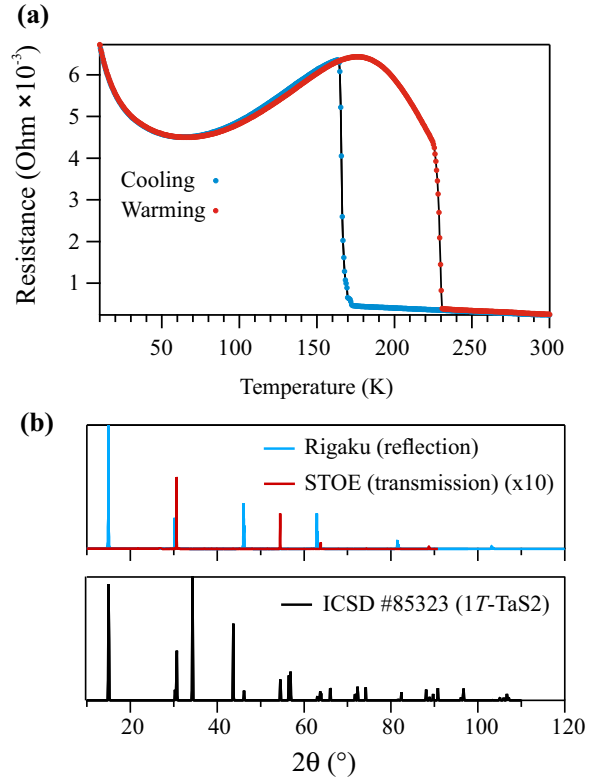


FIG. 6. (a) Resistance curve as a function of temperature during a cooling/warming cycle. The NCCDW to CCDW transition is clearly evident, as is the typically observed hysteresis upon warming. (b) (Upper curves) X-ray diffraction peaks obtained on a single crystal in both reflection and transmission geometries. (Lower curves) Reference spectra no. 85323, corresponding to the $1T$ -phase of TaS₂, from the Inorganic Crystal Structure Database (ICSD).

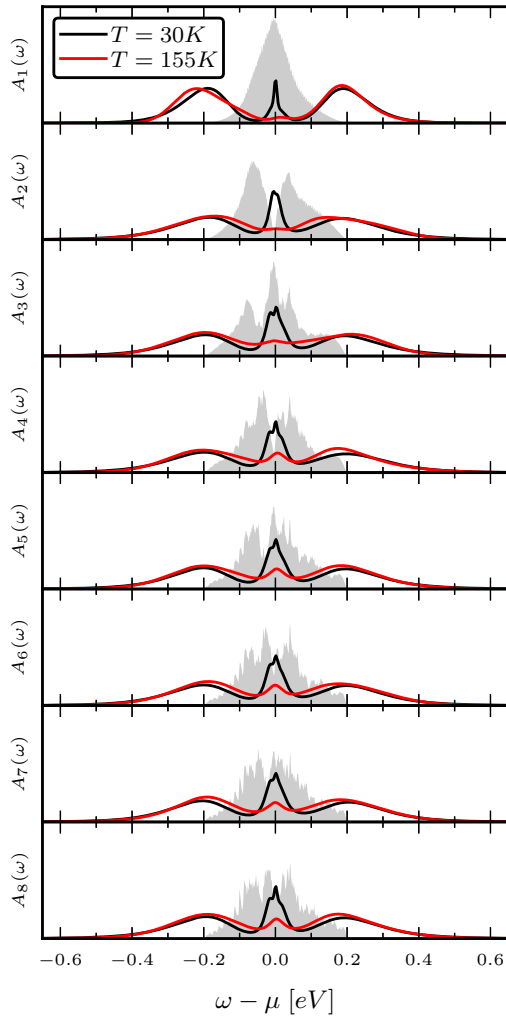


FIG. 7. Calculated spectral function $A_n(\omega)$ as a function of the layer index n for the L-type stacking described in the main text, with $n = 1$ being the surface layer. Grey solid curves are the noninteracting spectra obtained with DFT using the LDA. Black and red curves are the interacting spectra calculated with GW+EDMFT and are obtained at 30 K and 155 K respectively. The metallic quasiparticle peak is observed to extend into the bulk.

effectively strained lattice. Thereafter, dynamic cooling in this strained energy landscape could lead to the modified stacking configuration observed in experiments. This motivates future work on the dynamic nature of the interlayer behavior [65], both experimentally and theoretically. Independent of this discussion, our results expose the possibility of using uniaxial strain to create alternative protocols for inducing hidden phases.

IV. CONCLUSIONS

In summary, we have experimentally demonstrated that uniaxial strain induces a flat band with a collapsed gap in 1T-TaS₂, which appears below the CCDW transition temperature. The appearance of such a quasiparticle state within the CCDW gap is an indication of strong electronic correlations and Mott physics in strained TaS₂, which may have relevance for the

microscopic mechanisms governing the superconducting and metastable phases in this archetypal material. Our supporting GW+EDMFT calculations confirmed that a modification of interlayer coupling results in a strongly correlated state with a renormalized quasiparticle band and incoherent Hubbard band features. We postulate that the emergence of the narrow band occurs due to the reduced interlayer coupling compared with the equilibrium AL stacking in a manner similar to an L-stacked structure. Our observations validate strain as a parameter to control correlated behavior via interlayer coupling and highlight the potential of this approach for manipulating phase diagrams in layered systems.

ACKNOWLEDGMENTS

C.W.N., B.S., M.R., G.K., and C.M. acknowledge support from the Swiss National Science Foundation Grant No. P00P2_170597. F.P. and P.W. acknowledge support from the Swiss National Science Foundation through NCCR MARVEL and from the European Research Council through ERC Consolidator Grant No. 724103. C.W. and F.O.v.R. acknowledge the support from the Swiss National Science Foundation under Grant No. PCEFP2_194183 and by the Swedish Research Council (VR) through a neutron Project Grant Dnr. 2016-06955. The calculations were performed on the Beo05 clusters at the University of Fribourg and the Piz Daint cluster at the Swiss National Supercomputing Centre (CSCS) under Project ID mr26. We acknowledge DESY (Hamburg, Germany), a member of the Helmholtz Association HGF, for the provision of experimental facilities. Parts of this research were carried out at PETRA III and we would like to thank P. Glaweacke and M. v. Zimmermann for assistance in using beamline P21.1. Beamtime was allocated for Proposal No. I-20210288 EC. We thank M. Wolf and L. Rettig for providing constructive feedback on the manuscript. We gratefully acknowledge J. Chang for access to the Laue diffractometer at the University of Zurich, and Q. Wang for technical support obtaining Laue data. Skillful technical support was provided by M. Andrey, B. Hediger, G. Bächler and F. Bourqui. C. W. N. conceived the project. C. W. and F. O. v. R. fabricated the samples and performed the resistivity and diffraction measurements. ARPES and strain measurements were performed by C.W.N. and B.S. with assistance from M.R. and G.K., and were analysed by C.W.N. Electronic structure calculations were carried out by F.P. and P.W. XRD data was obtained by C.W.N., B.S., C.W., and O.I. The project was managed by C.W.N. together with C.M.C.W.N. wrote the manuscript with input from all authors.

APPENDIX: MATERIALS, METHODS, AND FURTHER DATA

Crystal growth. High quality single crystals of 1T-TaS₂ were grown by the chemical vapor transport (CVT) method using TaCl₅ as a transport agent. First, polycrystalline samples of 1T-TaS₂ were synthesized by mixing stoichiometric amounts of tantalum (powder, Alfa Aesar, 99.99%) and sulfur (pieces, Alfa Aesar, 99.999%) of a total mass of 1 g. The reactants were sealed in a quartz ampoule (l = 9 cm, diameter = 9 mm) under 1/3 atm. The quartz ampoule was heated to

1000 °C at a rate of 180 °C/h, kept at this temperature for four days and subsequently quenched in water. 200 mg of the synthesized powder and 10 mg TaCl₅ (anhydrous, powder, VWR, 99.999%) were sealed in a quartz ampoule ($l = 20$ cm, diameter = 7 mm) under vacuum and heated for six days in a two zone furnace in which the source zone and the growth zone temperatures and were fixed at 980 °C and 850 °C, respectively. Eventually, the tube was quenched in cold water to ensure the retaining of the 1T phase. The product was confirmed to be phase pure by powder x-ray diffraction (PXRD). Patterns were collected on an STOE STADI P diffractometer in transmission mode equipped with a Ge-monochromator using Cu K α 1 radiation and on a Rigaku SmartLab in reflection mode using Cu K α radiation. Transport measurements from 300 to 10 K were carried out with an excitation current of $I = 1$ mA on a Quantum Design Physical Property Measurement System (PPMS) Evercool with a 9-T magnet. Gold wires (25 μ m) were connected to the sample with silver epoxy in the standard four probe method.

Sample strain. Uniaxial strain was applied using a modified version of a previously described home-built strain cell [20], from which it was possible to reach 0.2% strain as measured by an electronic strain gauge in a Wheatstone bridge configuration. Samples to be prepared for straining were chosen to have large flat areas with minimal cracks or flakes at the surface as viewed under an optical microscope, in order to allow for more homogeneous strain application. Orientation of crystals was carried out using a commercial Laue diffractometer. Crystals were strained parallel to the a^* axis of the room-temperature phase. Bulk samples were initially cleaved with a scalpel to remove thicker layers, and then mounted onto the unstrained device and further thinned by Scotch tape cleaving. Unstrained and strained comparisons presented in this paper were obtained on the same crystal before and after straining. The data presented in Figs. 1 and 2 were obtained on different crystals. The strained and unstrained data are obtained on different cleaves and it is possible that the cleave plays a role in producing minor differences in the measured spectra. However, we emphasize that the band gap collapse has not previously been observed on unstrained samples, either in the literature or in our measurements. Spatial inhomogeneity in the surface cleave can lead to different spectral features near the Fermi level as shown in our recent paper (Ref. [44]). We note that these surfaces did not show the narrow band behavior collapsed band gap or the unusual temperature behavior

observed with strain. Hence cleave quality is unlikely to be the only factor involved.

ARPES. Photoemission measurements were carried out in a base pressure of 10^{-11} mbar. VUV photons with 21.2 eV were produced using a monochromatized He plasma source (SPECS GmbH). Low-energy UV photons were generated using a commercial optical setup (Harmonix, APE GmbH) generating tuneable output in the range 5.7–6.3 eV in non-linear crystals. Harmonic generation was driven by the output of a tuneable OPO pumped by a 532 nm Paladin laser (Coherent Inc) at 80 MHz. The beam polarization used was linear horizontal (s-pol) and the beam size was $80 \times 80 \mu\text{m}^2$. The sample surface was scanned by the encoded motion of a six-axis cryogenic manipulator (SPECS GmbH). Spectra were acquired using a Scienta-Omicron DA30 analyser. The energy resolution obtained from the Fermi edge of a polycrystalline Mo sample was 2.8 meV.

X-ray diffraction. Diffraction measurements were performed at the P21.1 beamline of the PETRA III synchrotron in a transmission geometry. Photons at 100 keV energy and linear horizontal polarization were selected. The beam profile was $1 \times 1 \text{ mm}^2$. The same design of strain cell was used as for the ARPES measurements, with a slit of material removed from the copper bridge to reduce the background copper signal.

Electronic structure calculations. The GW+EDMFT simulations were performed with the set-up described in Ref. [44], which considers eight 1T-TaS₂ layers and an embedding potential for the bulk. The local correlation and screening effects are treated with extended dynamical mean field theory (EDMFT) and the nonlocal ones at the GW level. We use a realistic band structure for the in-plane hopping [62] and interlayer hoppings $t_A = 0.2$ eV and $t_L = 0.045$ eV, which were optimized by comparing the local spectrum of the surface layer in the AL and LA stacked systems to the corresponding STM spectra [33]. In the L structure we use $t_L = 0.035$. Upon convergence, the GW+EDMFT calculation provides a momentum- and frequency-dependent self-energy $\Sigma_{ab}(k_{\parallel}, i\omega_n)$ and lattice Green's function $G_{ab}(k_{\parallel}, i\omega_n)$ with a, b layer indices and k_{\parallel} the in-plane momentum. The local spectral function $A_a = -\frac{1}{\pi} \text{Im} \frac{1}{N_{k_{\parallel}}} \sum_k G_{aa}(k_{\parallel}, \omega)$ is obtained with maximum entropy analytical continuation. The momentum-resolved spectra are obtained by Fourier-transforming the layer-resolved spectra with respect to the layer index [44].

- [1] C. Wu, D. Bergman, L. Balents, and S. Das Sarma, Flat bands and Wigner crystallization in the honeycomb optical lattice, *Phys. Rev. Lett.* **99**, 070401 (2007).
- [2] V. I. Iglovikov, F. Hébert, B. Grémaud, G. G. Batrouni, and R. T. Scalettar, Superconducting transitions in flat-band systems, *Phys. Rev. B* **90**, 094506 (2014).
- [3] D. C. Tsui, H. L. Stormer, and A. C. Gossard, Two-dimensional magnetotransport in the extreme quantum limit, *Phys. Rev. Lett.* **48**, 1559 (1982).
- [4] J. G. Bednorz and K. A. Müller, Possible high T_c superconductivity in the Ba-La-Cu-O system, *Z. Phys. B* **64**, 189 (1986).
- [5] Y. Cao, V. Fatemi, S. Fang, K. Watanabe, T. Taniguchi, E. Kaxiras, and P. Jarillo-Herrero, Unconventional

superconductivity in magic-angle graphene superlattices, *Nature (London)* **556**, 43 (2018).

- [6] Y. Cao, V. Fatemi, A. Demir, S. Fang, S. L. Tomarken, J. Y. Luo, J. D. Sanchez-Yamagishi, K. Watanabe, T. Taniguchi, E. Kaxiras *et al.*, Correlated insulator behaviour at half-filling in magic-angle graphene superlattices, *Nature (London)* **556**, 80 (2018).
- [7] S. Lisi, X. Lu, T. Benschop, T. A. de Jong, P. Stepanov, J. R. Duran, F. Margot, I. Cucchi, E. Cappelli, A. Hunter *et al.*, Observation of flat bands in twisted bilayer graphene, *Nat. Phys.* **17**, 189 (2021).
- [8] B. R. Ortiz, L. C. Gomes, J. R. Morey, M. Winiarski, M. Bordelon, J. S. Mangum, I. W. H. Oswald, J. A.

- Rodriguez-Rivera, J. R. Neilson, S. D. Wilson, E. Ertekin, T. M. McQueen, and E. S. Toberer, New kagome prototype materials: Discovery of KV_3Sb_5 , RbV_3Sb_5 , and CsV_3Sb_5 , *Phys. Rev. Mater.* **3**, 094407 (2019).
- [9] T. Neupert, M. M. Denner, J. X. Yin, R. Thomale, and M. Z. Hasan, Charge order and superconductivity in kagome materials, *Nat. Phys.* **18**, 137 (2022).
- [10] M. Kang, S. Fang, J. Yoo, B. R. Ortiz, Y. M. Oey, J. Choi, S. H. Ryu, J. Kim, C. Jozwiak, A. Bostwick *et al.*, Charge order landscape and competition with superconductivity in kagome metals, *Nat. Mater.* **22**, 186 (2023).
- [11] C. W. Hicks, M. E. Barber, S. D. Edkins, D. O. Brodsky, and A. P. Mackenzie, Piezoelectric-based apparatus for strain tuning, *Rev. Sci. Instrum.* **85**, 065003 (2014).
- [12] A. Steppke, L. Zhao, M. E. Barber, T. Scaffidi, F. Jerzembeck, H. Rosner, A. S. Gibbs, Y. Maeno, S. H. Simon, A. P. Mackenzie, and C. W. Hicks, Strong peak in T_c of Sr_2RuO_4 under uniaxial pressure, *Science* **355**, eaaf9398 (2017).
- [13] H. H. Kim, S. M. Souliou, M. E. Barber, E. Lefrançois, M. Minola, M. Tortora, R. Heid, N. Nandi, R. A. Borzi, G. Garbarino *et al.*, Uniaxial pressure control of competing orders in a high-temperature superconductor, *Science* **362**, 1040 (2018).
- [14] V. Grinenko, S. Ghosh, R. Sarkar, J. C. Orain, A. Nikitin, M. Elender, D. Das, Z. Guguchia, F. Brückner, M. E. Barber *et al.*, Split superconducting and time-reversal symmetry-breaking transitions in Sr_2RuO_4 under stress, *Nat. Phys.* **17**, 748 (2021).
- [15] Q. Wang, K. von Arx, D. G. Mazzone, S. Mustafi, M. Horio, J. Küspert, J. Choi, D. Bucher, H. Wo, J. Zhao *et al.*, Uniaxial pressure induced stripe order rotation in $La_{1.88}Sr_{0.12}CuO_4$, *Nat. Commun.* **13**, 1795 (2022).
- [16] M. Yankowitz, S. Chen, H. Polshyn, Y. Zhang, K. Watanabe, T. Taniguchi, D. Graf, A. F. Young, and C. R. Dean, Tuning superconductivity in twisted bilayer graphene, *Science* **363**, 1059 (2019).
- [17] J. Mao, S. P. Milovanovic, M. Andelkovic, X. Lai, Y. Cao, K. Watanabe, T. Taniguchi, L. Covaci, F. M. Peeters, A. K. Geim *et al.*, Evidence of flat bands and correlated states in buckled graphene superlattices, *Nature (London)* **584**, 215 (2020).
- [18] S. Riccò, M. Kim, A. Tamai, S. M. Walker, F. Y. Bruno, I. Cucchi, E. Cappelli, C. Besnard, T. K. Kim, P. Dudin *et al.*, In situ strain tuning of the metal-insulator-transition of Ca_2RuO_4 in angle-resolved photoemission experiments, *Nat. Commun.* **9**, 4535 (2018).
- [19] V. Sunko, E. Abarca Morales, I. Marković, M. E. Barber, D. Milosavljević, F. Mazzola, D. A. Sokolov, N. Kikugawa, C. Cacho, P. Dudin *et al.*, Direct observation of a uniaxial stress-driven Lifshitz transition in Sr_2RuO_4 , *npj Quantum Mater.* **4**, 46 (2019).
- [20] C. W. Nicholson, M. Rumo, A. Pulkkinen, G. Kremer, B. Salzmann, M.-I. Mottas, B. Hildebrand, T. Jaouen, T. K. Kim, S. Mukherjee *et al.*, Uniaxial strain-induced phase transition in the 2D topological semimetal $IrTe_2$, *Commun. Mater.* **2**, 25 (2021).
- [21] R. Noguchi, M. Kobayashi, Z. Jiang, K. Kuroda, T. Takahashi, Z. Xu, D. Lee, M. Hirayama, M. Ochi, T. Shirasawa *et al.*, Evidence for a higher-order topological insulator in a three-dimensional material built from van der Waals stacking of bismuth-halide chains, *Nat. Mater.* **20**, 473 (2021).
- [22] J. A. Wilson, F. J. Di Salvo, and S. Mahajan, Charge-density waves and superlattices in the metallic layered transition metal dichalcogenides, *Adv. Phys.* **24**, 117 (1975).
- [23] B. Sipos, A. F. Kusmartseva, A. Akrap, H. Berger, L. Forró, and E. Tutis, From Mott state to superconductivity in $1T-TaS_2$, *Nat. Mater.* **7**, 960 (2008).
- [24] L. Stojchevska, I. Vaskivskiy, T. Mertelj, P. Kusar, D. Svetin, S. Brazovskii, and D. Mihailovic, Ultrafast switching to a stable hidden quantum state in an electronic crystal, *Science* **344**, 177 (2014).
- [25] D. Cho, S. Cheon, K. S. Kim, S. H. Lee, Y. H. Cho, S. W. Cheong, and H. W. Yeom, Nanoscale manipulation of the Mott insulating state coupled to charge order in $1T-TaS_2$, *Nat. Commun.* **7**, 10453 (2016).
- [26] M. Klanjšek, A. Zorko, R. Žitko, J. Mravlje, Z. Jagličić, P. K. Biswas, P. Prelovšek, D. Mihailovic, and D. Arčon, A high-temperature quantum spin liquid with polaron spins, *Nat. Phys.* **13**, 1130 (2017).
- [27] E. Tosatti and P. Fazekas, On the nature of the low-temperature phase of $1T-TaS_2$, *J. Phys. Colloques* **37**, C4-165 (1976).
- [28] P. Fazekas and E. Tosatti, Electrical, structural and magnetic properties of pure and doped $1T-TaS_2$, *Philos. Mag. B* **39**, 229 (1979).
- [29] F. J. Di Salvo and J. E. Graebner, The low temperature electrical properties of $1T-TaS_2$, *Solid State Commun.* **23**, 825 (1977).
- [30] T. Ritschel, J. Trinckauf, K. Koepnik, B. Büchner, M. V. Zimmermann, H. Berger, Y. I. Joe, P. Abbamonte, and J. Geck, Orbital textures and charge density waves in transition metal dichalcogenides, *Nat. Phys.* **11**, 328 (2015).
- [31] T. Ritschel, H. Berger, and J. Geck, Stacking-driven gap formation in layered $1T-TaS_2$, *Phys. Rev. B* **98**, 195134 (2018).
- [32] S. H. Lee, J. S. Goh, and D. Cho, Origin of the insulating phase and first-order metal-insulator transition in $1T-TaS_2$, *Phys. Rev. Lett.* **122**, 106404 (2019).
- [33] C. J. Butler, M. Yoshida, T. Hanaguri, and Y. Iwasa, Mottness versus unit-cell doubling as the driver of the insulating state in $1T-TaS_2$, *Nat. Commun.* **11**, 2477 (2020).
- [34] J. Lee, K. H. Jin, and H. W. Yeom, Distinguishing a Mott insulator from a trivial insulator with atomic adsorbates, *Phys. Rev. Lett.* **126**, 196405 (2021).
- [35] P. A. Lee, N. Nagaosa, and X. G. Wen, Doping a Mott insulator: Physics of high-temperature superconductivity, *Rev. Mod. Phys.* **78**, 17 (2006).
- [36] K. Fung, J. Steeds, and J. A. Eades, Application of convergent beam electron diffraction to study the stacking layers in transition metal dichalcogenides, *Phys. B: Condens. Matter* **99**, 47 (1980).
- [37] S. Tanda, T. Sambongi, T. Tani, and S. Tanaka, X-ray study of charge density wave structure in $1T-TaS_2$, *J. Phys. Soc. Jpn.* **53**, 476 (1984).
- [38] M. B. Walker and R. L. Withers, Stacking of charge-density waves in $1T$ transition-metal dichalcogenides, *Phys. Rev. B* **28**, 2766 (1983).
- [39] K. Nakanishi and H. Shiba, Theory of three-dimensional orderings of charge density waves in $1T-TaX_2$ (X: S, Se), *J. Phys. Soc. Jpn.* **53**, 1103 (1984).
- [40] M. Naito, H. Nishihara, and S. Tanaka, Nuclear magnetic resonance and nuclear quadrupole resonance study of ^{181}Ta in the commensurate charge density wave state of $1T-TaS_2$, *J. Phys. Soc. Jpn.* **55**, 2410 (1986).

- [41] M. Bovet, S. van Smaalen, H. Berger, R. Gaal, L. Forró, L. Schlapbach, and P. Aebi, Interplane coupling in the quasi-two-dimensional $1T$ -TaS₂, *Phys. Rev. B* **67**, 125105 (2003).
- [42] K. Rossnagel and N. V. Smith, Spin-orbit coupling in the band structure of reconstructed $1T$ -TaS₂, *Phys. Rev. B* **73**, 073106 (2006).
- [43] Z. Wu, K. Bu, W. Zhang, Y. Fei, Y. Zheng, J. Gao, X. Luo, Z. Liu, Y. P. Sun, and Y. Yin, Effect of stacking order on the electronic state of $1T$ -TaS₂, *Phys. Rev. B* **105**, 035109 (2022).
- [44] F. Petocchi, C. W. Nicholson, B. Salzmann, D. Pasquier, O. V. Yazyev, C. Monney, and P. Werner, Mott versus hybridization gap in the low-temperature phase of $1T$ -TaS₂, *Phys. Rev. Lett.* **129**, 016402 (2022).
- [45] L. Perfetti, T. A. Gloor, F. Mila, H. Berger, and M. Grioni, Unexpected periodicity in the quasi-two-dimensional Mott insulator $1T$ -TaS₂ revealed by angle-resolved photoemission, *Phys. Rev. B* **71**, 153101 (2005).
- [46] K. Rossnagel, On the origin of charge-density waves in select layered transition-metal dichalcogenides, *J. Phys.: Condens. Matter* **23**, 213001 (2011).
- [47] A. S. Ngankeu, S. K. Mahatha, K. Guilloy, M. Bianchi, C. E. Sanders, K. Hanff, K. Rossnagel, J. A. Miwa, C. Breth Nielsen, M. Bremholm, and P. Hofmann, Quasi-one-dimensional metallic band dispersion in the commensurate charge density wave of $1T$ -TaS₂, *Phys. Rev. B* **96**, 195147 (2017).
- [48] L. Perfetti, P. A. Loukakos, M. Lisowski, U. Bovensiepen, H. Berger, S. Biermann, P. S. Cornaglia, A. Georges, and M. Wolf, Time evolution of the electronic structure of $1T$ -TaS₂ through the insulator-metal transition, *Phys. Rev. Lett.* **97**, 067402 (2006).
- [49] J. Dong and F. Ding, The epitaxy of 2D materials growth, *Nat. Commun.* **11**, 5862 (2020).
- [50] M. I. B. Utama, R. J. Koch, K. Lee, N. Leconte, H. Li, S. Zhao, L. Jiang, J. Zhu, K. Watanabe, T. Taniguchi *et al.*, Visualization of the flat electronic band in twisted bilayer graphene near the magic angle twist, *Nat. Phys.* **17**, 184 (2021).
- [51] Q. Stahl, M. Kusch, F. Heinsch, G. Garbarino, N. Kretschmar, K. Hanff, K. Rossnagel, J. Geck, and T. Ritschel, Collapse of layer dimerization in the photo-induced hidden state of $1T$ -TaS₂, *Nat. Commun.* **11**, 1247 (2020).
- [52] K. Bu, W. Zhang, Y. Fei, Z. Wu, Y. Zheng, J. Gao, X. Luo, Y. P. Sun, and Y. Yin, Possible strain induced Mott gap collapse in $1T$ -TaS₂, *Commun. Phys.* **2**, 146 (2019).
- [53] D. Cho, G. Gye, J. Lee, S. H. Lee, L. Wang, S. W. Cheong, and H. W. Yeom, Correlated electronic states at domain walls of a Mott-charge-density-wave insulator $1T$ -TaS₂, *Nat. Commun.* **8**, 1 (2017).
- [54] Q. Stahl, D. Chen, T. Ritschel, C. Shekhar, E. Sadrollahi, M. C. Rahn, O. Ivashko, M. v. Zimmermann, C. Felser, and J. Geck, Temperature-driven reorganization of electronic order in CsV₃Sb₅, *Phys. Rev. B* **105**, 195136 (2022).
- [55] Y. Hu, X. Wu, B. R. Ortiz, X. Han, N. C. Plumb, S. D. Wilson, A. P. Schnyder, and M. Shi, Coexistence of tri-hexagonal and star-of-David pattern in the charge density wave of the kagome superconductor AV₃Sb₅, *Phys. Rev. B* **106**, L241106 (2022).
- [56] E. Martino, A. Pisoni, L. Ćirić, A. Arakcheeva, H. Berger, A. Akrap, C. Putzke, P. J. Moll, I. Batistić, E. Tutiš, L. Forró, and K. Semeniuk, Preferential out-of-plane conduction and quasi-one-dimensional electronic states in layered $1T$ -TaS₂, *npj 2D Mater. Appl.* **4**, 7 (2020).
- [57] Y. D. Wang, W. L. Yao, Z. M. Xin, T. T. Han, Z. G. Wang, L. Chen, C. Cai, Y. Li, and Y. Zhang, Band insulator to Mott insulator transition in $1T$ -TaS₂, *Nat. Commun.* **11**, 4215 (2020).
- [58] W. Zhang, Z. Wu, K. Bu, Y. Fei, Y. Zheng, J. Gao, X. Luo, Z. Liu, Y. P. Sun, and Y. Yin, Reconciling the bulk metallic and surface insulating state in $1T$ -TaSe₂, *Phys. Rev. B* **105**, 035110 (2022).
- [59] Y. Chen, W. Ruan, M. Wu, S. Tang, H. Ryu, H.-Z. Tsai, R. Lee, S. Kahn, F. Liou, C. Jia *et al.*, Strong correlations and orbital texture in single-layer $1T$ -TaSe₂, *Nat. Phys.* **16**, 218 (2020).
- [60] N. Tian, Z. Huang, B. G. Jang, S. Guo, Y.-J. Yan, J. Gao, Y. Yu, J. Hwang, M. Wang, X. Luo *et al.*, Metal to Mott insulator transition in two-dimensional $1T$ -TaSe₂, [arXiv:2211.08114](https://arxiv.org/abs/2211.08114).
- [61] H. Lin, W. Huang, K. Zhao, S. Qiao, Z. Liu, J. Wu, X. Chen, and S. H. Ji, Scanning tunneling spectroscopic study of monolayer $1T$ -TaS₂ and $1T$ -TaSe₂, *Nano Res.* **13**, 133 (2020).
- [62] D. Pasquier and O. V. Yazyev, *Ab initio* theory of magnetism in two-dimensional $1T$ -TaS₂, *Phys. Rev. B* **105**, L081106 (2022).
- [63] T. Ritschel, J. Trinckauf, G. Garbarino, M. Hanfland, M. v. Zimmermann, H. Berger, B. Büchner, and J. Geck, Pressure dependence of the charge density wave in $1T$ -TaS₂ and its relation to superconductivity, *Phys. Rev. B* **87**, 125135 (2013).
- [64] C. W. Nicholson, A. Lücke, W. G. Schmidt, M. Puppin, L. Rettig, R. Ernstorfer, and M. Wolf, Beyond the molecular movie: Dynamics of bands and bonds during a photoinduced phase transition, *Science* **362**, 821 (2018).
- [65] J. Maklar, S. Dong, J. Sarkar, Y. A. Gerasimenko, T. Pincelli, S. Beaulieu, P. S. Kirchmann, J. A. Sobota, S. L. Yang, D. Leuenberger *et al.*, Coherent light control of a metastable hidden phase, *Sci. Adv.* **9**, eadi4661 (2023).